Proceedings of the ASME 2018 Dynamic Systems and Control Conference
DSCC2018
September 30 – October 3, 2018, Atlanta, Georgia, USA

DSCC2018-9057

REALIZING TRAJECTORY-BASED COMBUSTION CONTROL IN A HYDRAULIC FREE PISTON ENGINE VIA A FAST-RESPONSE DIGITAL VALVE

Chen Zhang[a], Zongxuan Sun[b]
Department of Mechanical Engineering
University of Minnesota, Twin Cities Campus
Minneapolis, MN 55455

ABSTRACT

Previously, the authors have proposed the concept of piston trajectory-based combustion control enabled by a free piston engine (FPE) and shown its advantages on both thermal efficiency and emissions performance. The main idea of this control method is to design and implement an optimal piston trajectory into FPE and optimizes the combustion performance accordingly. To realize the combustion control in practice, it is obvious that the design of the optimal trajectory should consider the dynamic behaviors of the FPE's actuation systems as well as variable load dynamics and fuels' chemical kinetics.

In this paper, a comprehensive model describing the operation of a hydraulic FPE fueled by diesel under HCCI combustion mode is developed. Such a high fidelity model includes four parts, i.e. the piston dynamics, the hydraulic dynamics, the thermodynamics and the fuel's chemical kinetics. Extensive simulation results are produced, showing that by varying the switching strategy of a fast-response digital valve, the hydraulic FPE can operate at different working loads in a stable manner. Additionally, analysis has been conducted to quantify the thermal efficiency as well as the frictional loss and throttling loss of the FPE. At last, a feedback control is developed to generate optimal switching strategies for the digital valve aimed to achieve the HCCI combustion phasing control. The resulted switching strategy of the digital valve not only increases the thermal efficiency by 0.76%, but also reduces frictional loss by 9.8%, throttling loss by 6.5% as well as NOx emission by 85.6%, which clearly demonstrates the effectiveness of the trajectory-based combustion control.

INTRODUCTION

Currently, increasing public attention is drawn to internal combustion engine (ICE) due to concerns about energy consumption and environmental impact. Many technologies have been proposed to solve it and the low-temperature combustion (LTC) is considered as a promising one to reduce fuel consumption and NOx emissions simultaneously [1-3]. However, the massive production of the related engines has not been achieved yet, mainly due to the lack of precise and robust ignition mechanism. Such mechanisms are difficult to achieve in a conventional ICE since the LTC is mainly driven by the chemical kinetics of the fuel and the thermodynamics of in-cylinder gases (dashed block in Fig. 1). The existing control methods in conventional ICE, including regulating exhaust gas recirculation [4, 5], variable valve timings [6, 7] and stratifying charge [8, 9], can only affect the chemical kinetics and in-cylinder gas dynamics in a cycle by cycle manner, rather than adjust them in real time.

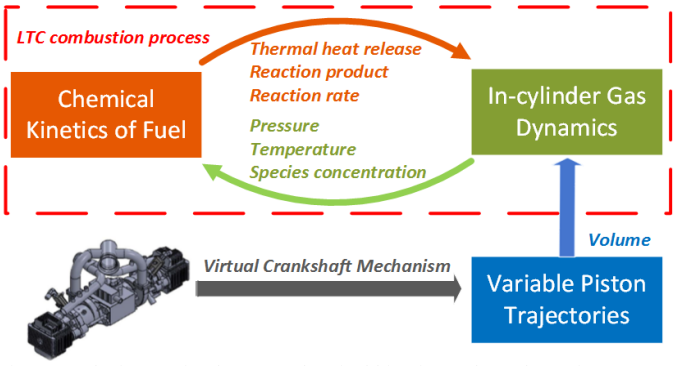

Figure 1. The interaction between chemical kinetics and gas dynamics

Free piston engine (FPE) is an alternative to ICE, which is also a promising platform to implement the LTC [10]. Due to the elimination of crankshaft, its piston can move freely and enables variable compression ratio (CR). On top of that, the flexibility of the FPE can even realize various piston motion patterns between the fixed top dead center (TDC) and the bottom dead center (BDC) points [11-13]. As a result, the

[a] Email: zhan2314@umn.edu
[b] Corresponding author, Email:zsun@umn.edu, Tel: 612-625-2107

interaction between the chemical kinetics and the in-cylinder gas dynamics can be adjusted actively through variable combustion chamber volume and the optimal combustion performance can be achieved, as shown in Fig. 1.

Enlightened by this observation, an advanced combustion control, namely the "Trajectory-based Combustion Control", has been proposed [11]. Its main idea is to utilize FPE's controllable piston trajectory as an additional control means to regulate the combustion chamber volume in real-time and adjust the in-cylinder gases pressure-temperature trace as well as species concentration prior, during and after the combustion. Under such a novel framework, the trajectory-based combustion control is capable of increasing the engine thermal efficiency significantly and reducing the engine-out emissions simultaneously [12]. Furthermore, since the FPE can vary its operational CR freely, the trajectory-based combustion control can be extended to almost all kinds of fuels, including renewable ones [13].

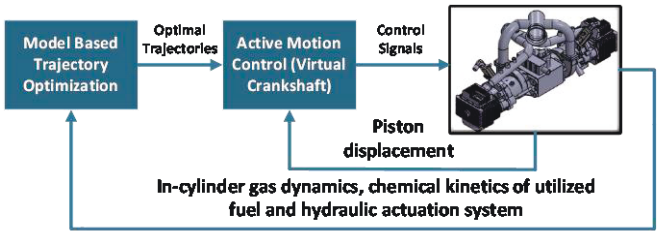

Figure 2. The overall configuration of trajectory-based combustion control

In this way, the piston trajectory of the FPE becomes a control variable that needs to be optimized according to real-time loads, properties of the fuel and the dynamics of the actuation system in the FPE. The overall system configuration of the trajectory-based combustion control is shown in Fig. 2, which includes two control loops. The inner loop is the piston motion control, which is achieved by the "Virtual Crankshaft" mechanism [14, 15]. Such a mechanism, based on the principle of robust repetitive control, has been developed and implemented on a prototype hydraulic FPE, enabling the FPE to track any periodic references accurately. The outer loop is the model-based trajectory optimization that generates the desired trajectory reference for the inner loop.

Previously, the outer loop has been investigated, while neglecting the hydraulic actuation system in the FPE [16]. In this sense, the corresponding reference may not be feasible in practice due to the limited capabilities of the hydraulic actuation system. It is also possible that the consumed hydraulic power realizing the trajectory reference outweighs the energy gain from the optimal combustion control. To overcome these challenges, the model-based trajectory optimization needs to consider the dynamic behavior of the hydraulic actuation system and thus a high fidelity model, which includes the hydraulic dynamics, the piston dynamics, the thermodynamics and the fuel's chemical kinetics, is required.

Such a model is developed and presented in this paper. The rest of this paper is organized as follow: the dynamics model based on the hydraulic FPE at the University of Minnesota is described at first. The simulation results from the model as well as the corresponding efficiency and losses analysis are presented afterward. Besides, a feedback control is developed aimed to achieve the optimal switching strategy for the digital valve to enhance the thermal efficiency of the combustion and reduces the frictional and throttling losses as well as the NOx emission. Finally, the advantages of the developed model and the related future work are concluded.

MODEL APPROACH

A dynamic model is first developed to describe the operation of the FPE fueled by diesel under HCCI combustion mode. Fig. 3 shows the picture and the schematics of the FPE. It has an opposed-piston opposed-cylinder (OPOC) design, which offers the highest power density and scavenging efficiency [14]. Two piston pairs exist in the FPE, namely the outer and the inner piston pairs. At each end, one outer piston and one inner piston, as well as the cylinder around them, form a combustion cylinder. Due to the symmetric structure, the TDC point of the left combustion cylinder is also the BDC point of the right combustion cylinder and vice versa. Thus, combustions occur inside each cylinder alternatively.

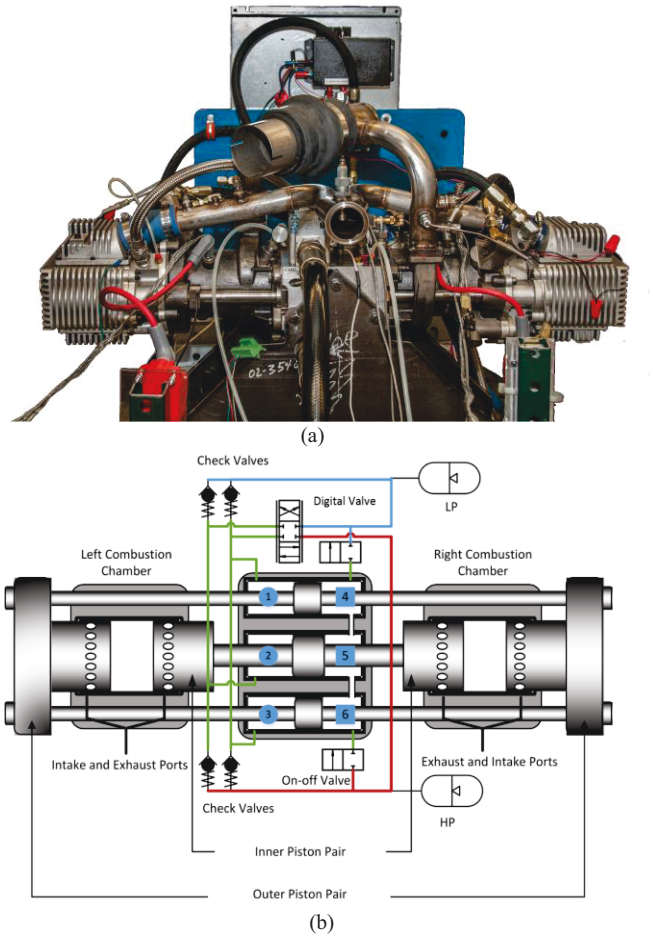

(a)

(b)

Figure 3. (a) Picture and (b) schematic of the prototype hydraulic FPE at the University of Minnesota

The hydraulic block lays between the two combustion cylinders and includes six hydraulic chambers as shown in Fig. 3 (b). Chambers 1 and 3 are connected and named as an *outer hydraulic chamber*, while the Chamber 2 as the *inner hydraulic chamber*. As can be seen, each hydraulic chamber is connected to a servo valve, whose opening controls the connection of the corresponding hydraulic chamber to either the high-pressure (HP) load or low-pressure (LP) tank. Chambers 4, 5 and 6 are interconnected to each other and forms the *synchronization chamber*, which synchronizes the pistons motions via two on-off valves.

In order to take all the above dynamic behaviors into consideration, the entire control-oriented model includes 4 parts, namely the piston dynamics, hydraulic dynamics, thermodynamics, and chemical kinetics.

A. Piston Dynamics

Piston dynamics of the FPE is governed by the in-cylinder gases force, the hydraulic force and the friction forces through the Newton second law, as shown in the free body diagram in Fig. 4 and equation (1) as below.

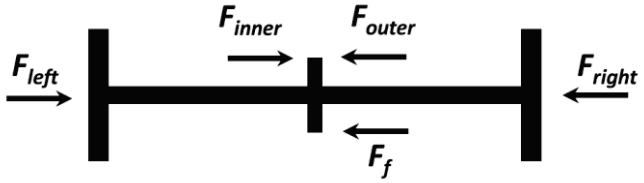

Figure 4. Free body diagram of the FPE's lumped piston pair

$$\begin{aligned}\ddot{x} &= \frac{1}{M}(F_{left}(x,\dot{x}) - F_{right}(x,\dot{x}) - F_f(\dot{x}) - F_{hyd}(\dot{x})) \\ &= \frac{1}{M}(F_{net}(x,\dot{x}) - F_f(\dot{x}) - F_{hyd}(\dot{x}))\end{aligned} \tag{1}$$

where x, $\dot{x}$ and $\ddot{x}$ are the displacement, velocity, and acceleration of the piston. M is the piston mass. F_{left}, F_{right}, and F_{net} are the left, right and net in-cylinder gases force, respectively, which can be calculated through the combustion cylinder pressure P and combustion piston area A_g. F_{hyd} is the net hydraulic force determined by the hydraulic pressure in each hydraulic chamber. F_f is the friction force, which is shown as:

$$F_f(\dot{x}) = -k_v \cdot \dot{x} \tag{2}$$

where k_v is the friction coefficient.

B. Hydraulic Dynamics

From Fig. 3 (b), the hydraulic chambers 1, 2 and 3 on the left side are connected to either the HP or LP through the check valve and/or the digital valve, whereas the three right hydraulic chambers 4, 5 and 6 are interconnected and serve as the synchronization mechanism. For the sake of convenience, the two piston pairs are assumed synchronized all the time. Thus, it only needs to derive the rate of pressure in all the three left chambers, which can be represented as follow:

$$\dot{P}_{left} = \frac{\beta}{V_{left}}(Q_{piston} + Q_{digital} + Q_{check}) \tag{3}$$

where $\dot{P}_{left}$ is the hydraulic pressure rate of each left chamber, β is the bulk modulus of the fluid, V_{left} is the specific volume of each left chamber. Q_{piston} is the flow caused by the piston motion, $Q_{digital}$ represents the flow through the digital valve and Q_{check} shows the flow through the check valve.

Based on the velocity of the piston, Q_{piston} can be derived:

$$Q_{piston} = A_h \cdot \dot{x} \tag{4}$$

where A_h is the hydraulic piston area.

The flow rate through the digital valve $Q_{digital}$ is more complicated to achieve. Let's take the hydraulic chamber 1 as an example. When the digital valve is in its bottom position, the chamber 1 is connected to the HP and the corresponding flow rate $Q_{digital}$ is:

$$Q_{digital} = C_d A_{ori} \cdot sign(P_{HP} - P_{left}) \cdot \sqrt{\frac{2 \cdot abs(P_{HP} - P_{left})}{\rho_{fluid}}} \tag{5}$$

where C_d is the discharge coefficient of the digital valve and the A_{ori} is the corresponding orifice area, P_{HP} is the pressure of the HP. ρ_{fluid} is the density of the hydraulic oil.

When the digital valve switches to its top position, the chamber 1 is connected to the LP and $Q_{digital}$ should be:

$$Q_{digital} = C_d A_{ori} \cdot sign(P_{left} - P_{LP}) \cdot \sqrt{\frac{2 \cdot abs(P_{left} - P_{LP})}{\rho_{fluid}}} \tag{6}$$

In addition, the digital valve is considered as a second order system, of which related details can be found in [16].

At last, as the flow through the check valve, Q_{check}, should only be considered if the pressure difference between the two sides of the check valve is larger than a prescribed threshold P_{check}. Let's take the hydraulic chamber 1 as an example again, if the pressure in the chamber 1 is already higher than the pressure of the HP plus the pressure threshold, then the check valve opens and Q_{check} is derived:

$$Q_{check} = -C_{d\_chcek} A_{check} \cdot \sqrt{\frac{2 \cdot (P_{left} - P_{HP})}{\rho_{fluid}}} \tag{7}$$

where C_{d_check} is the discharge coefficient of the check valve and the A_{check} is the corresponding orifice area.

On the other hand, if the pressure in the chamber 1 is lower than the pressure of the LP minus the pressure threshold, then the corresponding Q_{check} is:

$$Q_{check} = C_{d\_chcek} A_{check} \cdot \sqrt{\frac{2 \cdot (P_{LP} - P_{left})}{\rho_{fluid}}} \tag{8}$$

C. Thermodynamics

The thermodynamics part is developed based on the first thermodynamics law for a closed system since the scavenging process is neglected. Both the combustion cylinder pressure P and temperature T are derived herein. Such a derivation requires the information of each species concentration $[X_i]$ in the reaction mechanism, which will be described next.

1) Pressure rate equation

From the ideal gas law, the pressure P and its time derivative term are derived as below: (R is the universal gas constant)

$$P = \sum_i [X_i] \cdot R \cdot T \tag{9}$$

$$\dot{P} = P \sum_i [\dot{X}_i] / \sum_i [X_i] + P\dot{T}/T \tag{10}$$

2) Temperature rate equation

The temperature T is derived from the first law of the thermodynamics and the ideal gas law.

The first law of thermodynamics for a closed system is:

$$\frac{d(mu)}{dt} = -\dot{Q} - \dot{W} \tag{11}$$

where m is the total mass in the cylinder, u is the specific internal energy of the in-cylinder gas, $\dot{Q}$ is the heat transfer rate and $\dot{W}$ is the expansion work rate.

Furthermore, the heat transfer in this simulation is considered as a convection process, which can be achieved through a modified Woschini correlation [17].

Besides, the rate of expansion work is calculated as:

$$\dot{W} = P\dot{V} \tag{12}$$

where V is the combustion chamber volume, which is determined by the piston trajectory.

Now, given the fact that the specific enthalpy h can be obtained from the specific internal energy u:

$$h = u + Pv \tag{13}$$

where v is the specific volume of the in-cylinder gas.

Combining (11) and (13) together and used the closed system assumption, the following equation can be obtained:

$$\frac{d(mh)}{dt} = \dot{P}V - \dot{Q} \tag{14}$$

On the other hand, the total enthalpy of the in-cylinder gas can also be derived as the sum of each species enthalpy:

$$m \cdot h = \sum_i N_i \cdot \hat{h}_i \tag{15}$$

where N_i is the moles number of species i and $\hat{h}_i$ is mole-based specific enthalpy of species i. Furthermore, the rate of $\hat{h}_i$ can be calculated as:

$$\dot{\hat{h}}_i = c_{p,i}(T)\dot{T} \tag{16}$$

where $c_{p,i}(T)$ is the mole-based constant-pressure heat capacity of species i at temperature T, which can be achieved through the chemical kinetics part.

Combining (14), (15) and (16), the temperature rate $\dot{T}$ is derived as:

$$\dot{T} = \frac{-\sum_i [\dot{X}_i]\hat{h}_i - \dot{V}\sum_i [X_i]\hat{h}_i / V + P\sum_i [\dot{X}_i] / \sum_i [X_i] - \dot{Q}/V}{\sum_i [X_i] c_{p,i}(T) - P/T} \tag{17}$$

D. Chemical Kinetics

The chemical kinetics part offers important information, such as the values of $c_{p,i}(T)$ and $\hat{h}_i$ as well as each species concentrations $[X_i]$, to complete the model development.

The thermodynamic properties of each species, e.g. $c_{p,i}(T)$ and $\hat{h}_i$, are listed as the function of T in the reaction mechanism via the NASA polynomial parameterization [18].

The history of each species concentration $[X_i]$ can be derived via integrating the differential equation as below:

$$[\dot{X}_i] = \frac{d}{dt}\left(\frac{N_i}{V}\right) = \frac{\dot{N}_i}{V} - \frac{\dot{V}N_i}{V^2} = w_i - \frac{\dot{V}}{V}[X_i] \tag{18}$$

where w_i is the production rate of species i from the reaction.

In order to reduce computational time and keep sufficient chemical kinetics information for the subsequent optimization, a unique phase separation method has been proposed previously [19] and is employed in this study. In this method, an engine cycle is separated into four phases and a specific reaction mechanism with the minimal size is applied in each phase to represent the corresponding chemical kinetics as precisely as possible. The general idea of the phase separation method will be described briefly below and the detailed information can be found in [19].

Phase 1: This phase begins from the BDC point to the time instant when T reaches 500K. Such a low temperature makes few reactions proceeding and thus no reaction mechanism is applied here.

Phase 2: A simplified reaction mechanism is employed in this phase to represent the ignition process of the diesel until all the fuel molecules are converted into CO and H_2:

$$R_1 : C_{10.8}H_{18.7} + 5.4O_2 \rightarrow 10.8CO + 9.35H_2$$

where its reaction rate is calibrated based on a detailed reaction mechanism as shown in [20]:

$$RR_1 = 4.83 \times 10^9 \cdot [C_{10.8}H_{18.7}]^{0.1} \cdot [O_2]^{1.65} \exp\left(-\frac{14200}{T}\right) \tag{19}$$

Phase 3: afterward, the CO and H_2 are converted to final products CO_2 and H_2O and release the majority of thermal energy. The employed reaction mechanism is shown below:

$$R_2 : CO + H_2O \rightarrow CO_2 + H_2$$

$$_3R \quad _2H + 0.5 \quad _2O \rightarrow \quad _2O$$

where the corresponding reaction rates are derived as [21]:

$$RR_2 = 2.75 \times 10^9 \cdot [CO] \cdot [H_2O] \exp\left(-\frac{10065}{T}\right) \tag{20}$$

$$RR_3 = 1.5\times10^9 \cdot [H_2][O_2]^{0.5} \exp(-\frac{17609}{T}) \quad (21)$$

Sub-phase: when the temperature is over 1800K, the production of NOx should be taken into account. The thermal NOx generation mechanism is added here since it is the most suitable mechanism for high temperature and rich oxygen environment. By kinetic analysis, an overall expression for the rate of thermal NOx formation is derived and modified from Bowman et al [22].

Phase 4: after the T decreases to 900K, almost all the reaction products remain constants and there is no need to consider the chemical kinetics any further.

Key parameters used in the model are listed in Table I.

TABLE I. KEY MODELING PARAMETERS OF FREE PISTON ENGINE

Parameter	*Description*	*Value*
A_g	combustion piston area	0.002 m^2
A_h	hydraulic piston area	1.41×10^{-4} m^2
A_{ori_max}	digital valve maximum orifice	1.90×10^{-5} m^2
A_{check}	check valve orifice	5.50×10^{-5} m^2
C_d	digital valve discharge coefficient	0.7
C_{d_check}	check valve discharge coefficient	0.7
D_p	hydraulic chamber diameter	20mm
k_v	friction coefficient	40
Lp	piston length	66mm
M	piston pair mass	15 kg
P_{check}	check valve crack pressure	20×10^5 Pa
R	gas constant	287.035 J/kg-K
β	hydraulic oil bulk modulus	1.0×10^9 Pa
ρ_{fluid}	hydraulic oil density	870 kg/m^3
x_{in}	the position of the intake port	52 mm
Q_{LHV}	low heating value of the fuel	45.6 MJ/kg
C_v	constant volume heat capacity	719 J/kg.
R_u	universal gas constant	8.314 J/mol/K

SIMULATION RESULTS

Fig. 5 shows the stable combustion performance of the modeled hydraulic FPE at three different working loads, which is powered by three fuel injection amounts, i.e. 10.2 mg, 6.7mg and 3.8mg respectively. In these cases, the simulated pressure of the HP is fixed at 5000 psi, while the pressure of the LP is at 200 psi. In addition, the hydraulic FPE first goes through a motoring process (from the initial time to 50ms), while the existing fluid power in the HP is used to move the piston of the FPE back and forth until it reaches the desirable CR = 17 to trigger the HCCI combustion subsequently.

It should be noted that such a stable combustion performance can only be achieved after a thorough calibration on the switching strategy of the digital valve due to the dynamic coupling of the piston motion and the combustion kinetics. In other words, a feedforward control is developed offline for the digital valve switching aimed to regulate the piston motion according to various fuel injection amount.

The feedforward control is more obvious from Fig. 6, which is a zoomed-in figure of Fig. 5 during a specific time duration.

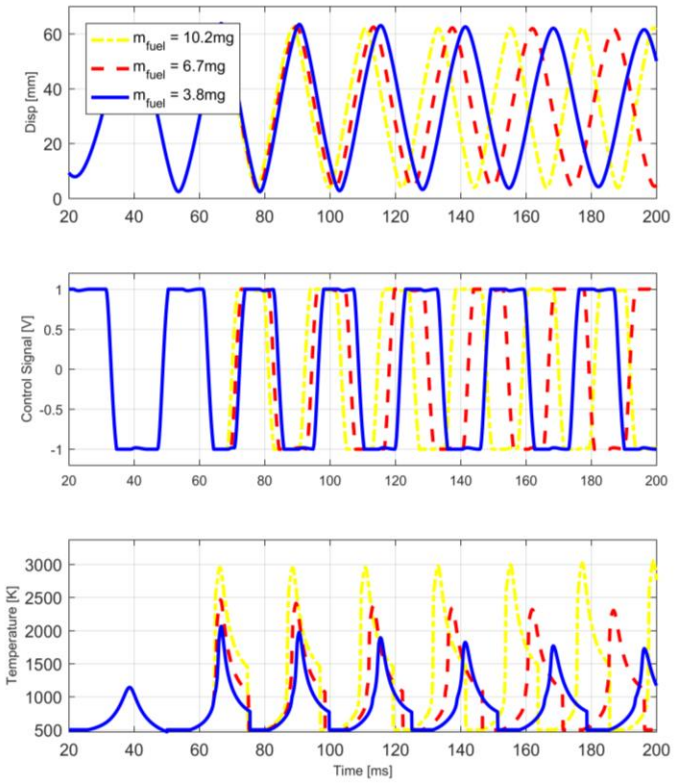

Figure 5. Operation of the hydraulic FPE at different loads, from the top to the bottom showing displacement of the right combustion cylinder, the control signal of the digital valve and temperature in the left combustion cylinder

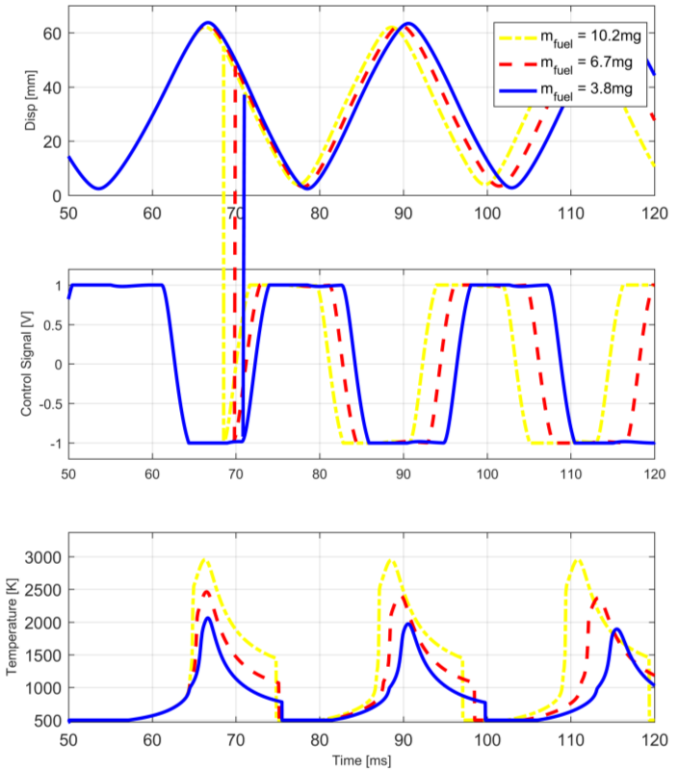

Figure 6. Zoomed in the figure of Fig. 5 from 50ms to 120ms

Clearly, around 65ms, all the pistons in three case are at their own end point simultaneously (the TDC point from the perspective of the left combustion cylinder). However, in order to sustain the piston motion, the 10.2mg case should switch the digital valve at 55 mm. In the 6.7mg case, the switching of the digital valve needs to wait for a while until the piston reaches 50 mm, as shown in the red dashed lines. The switching time of digital valve for the 3.8mg case is even longer, while the piston has to reach 45mm and then switch the valve, as shown in the blue solid lines in Fig. 6.

From the above observation, it can be concluded that the stable combustion performance of the hydraulic FPE can only be achieved by carefully organizing the fuel injection amount with the digital valve switching strategy. Fig. 7 shows such a calibrated look-up table for the digital valve switching at various working loads.

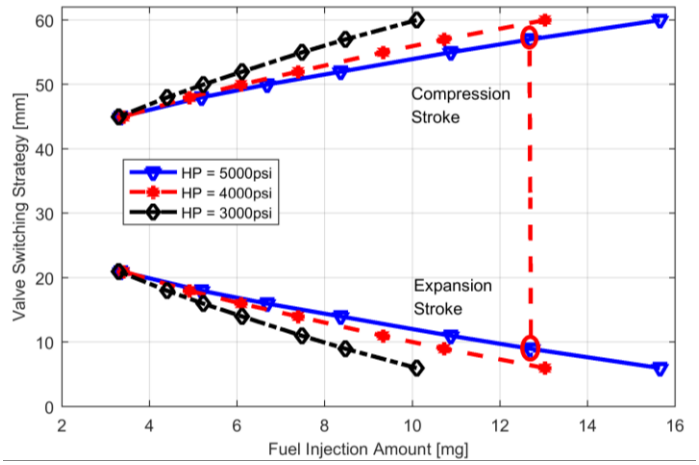

Figure 7. Piston displacement based switching strategy of the digital valve to achieve stable operation of the hydraulic FPE at various loads. (compression stroke and expansion stroke refer to right combustion cylinder)

In Fig. 7, the points on the top lines refer to the digital valve switching locations during the compression stroke, while the points at the bottom lines refer to the switching locations during the expansion stroke. It should be noted that the pairs of the valve switching locations refer to the two strokes have to be selected simultaneously to ensure the hydraulic FPE operating in a stable manner. As an example, assuming the hydraulic FPE operating at HP = 5000psi with fuel injection amount equals 12.6mg, then the pair of the digital valve switching strategy should be selected accordingly, as shown in the red circles.

In addition, it is obvious that higher working load, indicating by both higher fuel injection amount and higher pressure in HP, requires the digital valve switching at the lower position during the expansion stroke and higher position during the compression stroke. Enlightened by Fig. 6, such an action actually increases resistance during each stroke and thus provide more output flow as demand. When the fuel injection amount is reduced at a specific pressure, indicating lower working load is demanded, the digital valve switching strategy is varied accordingly by increasing the switching location during the expansion stroke and reducing the location during the compression stroke.

Besides, as can be seen in Fig. 7, the range of the available fuel injection amount also depends on the pressure of the HP. By operating at a higher pressure of HP (5000 psi), the range of the available fuel injection amount (from 3.5 mg to 15.8mg) is much larger than the case with the lower pressure of HP (3000psi), which is only in the range of 3.5mg to 10mg. If large fuel injection amount is utilized in low-pressure case, the aggressive combustion force cannot be resisted sufficiently by hydraulic forces. As a result, the piston will move towards the physical limitation of the FPE and cause collision eventually.

EFFICIENCY ANALYSIS

Fig. 8 shows the thermal efficiency of the combustion, the friction losses as well as the throttling losses in the hydraulic FPE at different working loads.

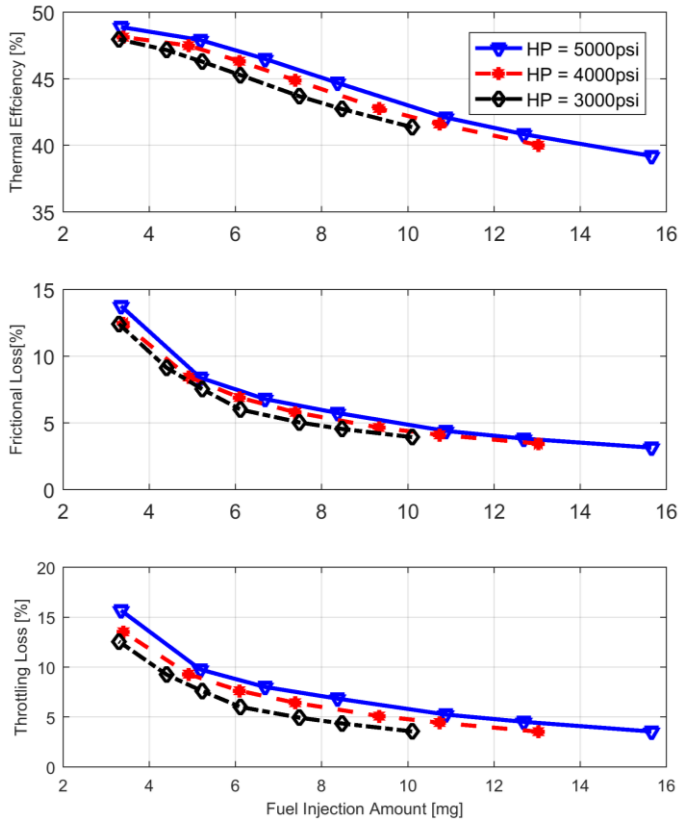

Figure 8. Efficiency analysis of the hydraulic FPE at different working loads, including thermal efficiency, friction losses, and throttling losses

Thermal efficiency: It is obvious that the majority of the FPE's thermal efficiency is higher than 40%. This is intuitive since the FPE can always operate at relatively higher CR (CR is around 17 in these cases) due to the elimination of the mechanical crankshaft. On the other hand, the HCCI combustion mode can also improve the thermal efficiency since the combustion duration is relatively short, enabling the combustion process to be closer to the ideal Otto cycle.

In addition, the thermal efficiency of the combustion at lower working load (around 50% in most cases) is higher than its counterpart at higher working load cases. The main reason for this variation is caused by more significant heat losses in latter cases due to the richer air-fuel mixture and much higher temperature after the combustion. Besides, higher CR is employed at lower load to facilitate the ignition of the lean air-fuel mixture and thus improves its thermal efficiency as well.

Friction losses: In the entire working load domain, the friction losses (less than 14%) are always relatively small compared to the losses in conventional ICE. This advantage is attributed to the unique characteristics of the hydraulic FPE. Compared to conventional ICE, the hydraulic FPE possesses much fewer components, which significantly reduces the friction. On top of that, the side force around the FPE's piston is much smaller due to its linear piston motion and therefore further reduces the friction losses.

Furthermore, the friction losses are higher in low working load cases since the higher CR increases the FPE operation frequency in these cases and thus generates higher mean piston speed.

Throttling losses: In addition, the throttling loss is also relatively small compared to the conventional hydraulic pump. It is because of the utilization of the fast response digital valve in the hydraulic FPE. Since the digital valve can open fully at two ends, the throttling loss only occurs when the valve switches from one end to the other. Due to the fast response of the valve, such a loss is reduced as small as possible.

The third row of Fig. 8 clearly shows that the throttling losses are higher at lower load. It is because that the digital valve switches at the center part of the stroke in these cases, while the piston speed is relatively higher. At high working load, the digital valve switches at location closed to end points and therefore lower piston speed. Similarly, the lower pressure of the HP generates less throttling losses at specific fuel injection amount since the digital valve switching strategy is closer to end points of each stroke in lower HP pressure cases.

HCCI COMBUSTION PHASING CONTROL

In this section, an HCCI combustion phasing control is presented, which combines the previous look-up table and a stroke-by-stroke feedback control based on the location of the heat release. The related block diagram is shown in Fig. 9.

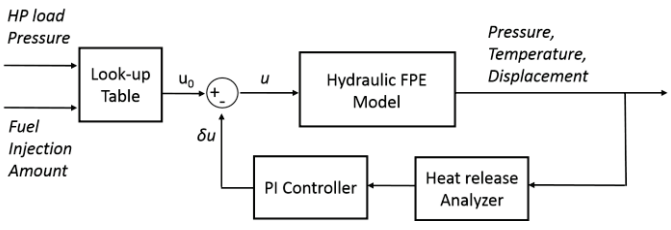

Figure 9. Block diagram of the feedback control on HCCI combustion phase in the hydraulic FPE

As can be seen in Fig. 9, the switching strategy of the digital valve u is achieved by two parts. The first part comes from the previously generated look-up table. By given the load pressure of HP and the targeted fuel injection amount, the original u_0 is found to ensure the hydraulic FPE is operating in a stable manner. In this study, the developed look-up table can deal with 1 mg disturbance on the fuel injection amount. It should be note that such a stability also depends heavily on the FPE's working condition. For example, higher intake temperature as well as higher working loads can further improve the FPE's stability. The second part is achieved by calculating the time instant when 50% chemical energy has been released through a heat release analyzer [19]. Afterward, such a time instant is compared to the time instant when the piston reaches the TDC point in a combustion cycle to realize the ideal Otto cycle and reduce the ringing intensity [19]. The variation between these two time instants will be sent to a PI controller, which calculates the feedback portion δu accordingly. It should be noted herein that u actually represents two switching locations of the digital valve during the expansion stroke and compression stroke respectively, as shown in Fig. 7. As a result, the adjustment δu also represents such a pair, while the phasing error in right combustion cylinder provides the adjustment for the expansion stroke and the phasing error in left combustion cylinder offers the adjustment for the compression stroke.

The effectiveness of the HCCI combustion phase control is shown in Fig. 10 evidently, which represents two specific combustion cycles before and after the feedback control. The base case herein represents the operation performance of the hydraulic FPE with 6.7mg fuel injection amount under the pressure of HP equals 5000psi.

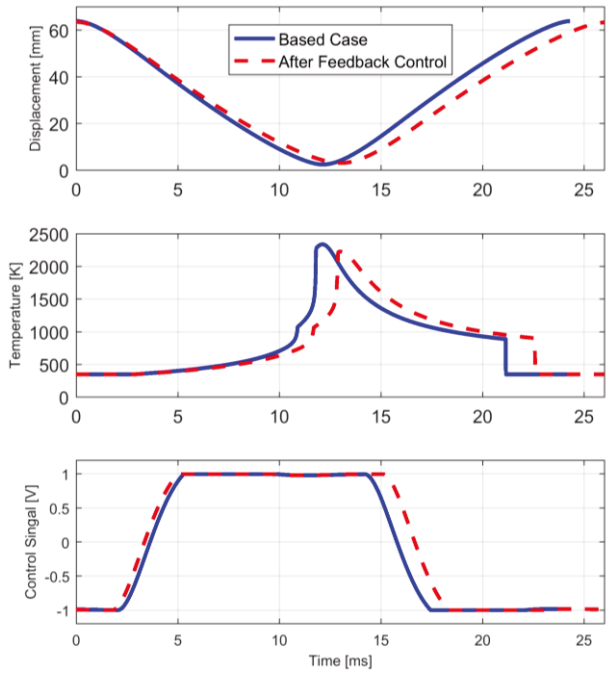

Figure 10. Two combustion cycles before and after the feedback combustion phase control. From the top to the bottom are piston displacement, the temperature of the right combustion cylinder and control signal of digital valve

As can be seen in Fig. 10, through the feedback combustion phasing control, the digital valve slightly advances its switching points during both compression and expansion strokes. As a result, the after-control case extends the period of the combustion cycle, reduces the corresponding CR and thus locates the major heat release time closer to its own TDC point. From the temperature profile, the related heat loss for the after-control case is less compared to the base case due to the shorter duration of the high-temperature environment around the TDC point inside the combustion cylinder.

The chemical kinetics of the air-fuel mixtures for these two cases show the longer ignition delay in the after-control case more clearly, as can be seen in Fig. 11. It is obvious from the diesel, CO and H_2 mass profiles that the first ignition delay in the after-control case is postponed by almost 0.9ms due to the adjustment of the piston trajectory caused by different valve switching strategy. Due to this delay, the second ignition delay is also postponed by 1.0ms in the after-control case, as shown in CO_2 and H_2O mass profiles.

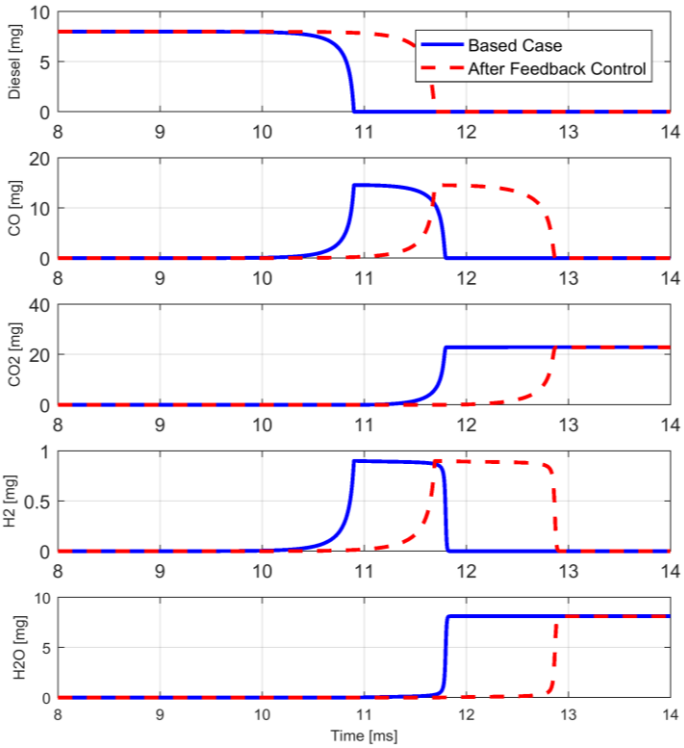

Figure 11. The chemical kinetics of two combustion cycles before and after the feedback combustion phase control. From the top to the bottom are the mass histories of Diesel, CO, CO_2, H_2, and H_2O respectively.

The detailed comparison between these two cases is also listed in Table II. Clearly, with the feedback phasing control, not only the thermal efficiency of the combustion is enhanced due to more appropriate combustion phasing, but the friction loss, as well as the throttling losses, are also reduced due to slower piston speed and closer valve switching location to end points of trajectory. On top of that, even the NOx emission is decreased after the feedback control due to the lower peak temperature in the combustion cylinder, as shown in the second row of the Fig. 10. Such a comparison evidently demonstrates the effectiveness of the trajectory-based combustion control enabled by FPE that by implementing an appropriate piston trajectory via an appropriate digital valve switching strategy, the optimal operational performance of the FPE can be achieved in terms of higher thermal efficiency, reduced friction and throttling losses and fewer emissions.

TABLE II. FPE PERFORMANCE COMPARISON BEFORE AND AFTER THE COMBUSTION PHASE CONTROL

Characteristics	*Base Case*	*After-Control Case*
TDC point (ms)	12.08	13.05
Heat Release Time (ms)	11.81	12.94
Thermal Efficiency (%)	47.35	47.71
Friction loss (%)	7.74	6.98
Throttling loss (%)	8.34	7.80
NOx emission (mg)	145.28	20.91

CONCLUSION

In this paper, a dynamics model representing the operation of a hydraulic FPE under HCCI combustion mode was developed. In order to enhance the fidelity of the model, the thermodynamics within the combustion cylinders, the chemical kinetics of diesel fuel, the dynamics of the hydraulic actuation system as well as the corresponding piston dynamics are considered. Extensive simulation results are obtained, which shows that by regulating the switching time of the digital valve according to the fuel injection amount, the hydraulic FPE can operate in a stable manner. A comprehensive efficiency analysis is also conducted, showing that higher thermal efficiency of the combustion as well as lower friction and throttling losses can be achieved due to the unique characteristics of the FPE architecture. At last, a feedback control is developed, which combines the generated look-up table with the information of the HCCI combustion phasing from the previous stroke and fine turns the switching strategy of the digital valve. Such a control method demonstrates the effectiveness of the piston trajectory-based combustion control clearly in terms of higher thermal efficiency, reduced friction losses as well as throttling losses and decreased NOx emission.

In the future, a model-based optimization will be developed based on the presented model in this paper. Both online and offline algorithms will be considered to eventually realize the implementation of the piston trajectory-based HCCI combustion control in a prototype FPE.

ACKNOWLEDGMENT

This study is supported by National Science Foundation (NSF) under grant CMMI-1634894.

REFERENCES

[1] Onishi, S.,Han Jo, S., Shoda, K., Do Jo, P. and Kato, S., 1979, "Active Thermo-Atmosphere Combustion (ATAC): A New Combustion Process for Internal Combustion Engine," SAT Technical Paper Series, Paper NO. 790501

[2] Zhao, F., Asmus, T. W., Assanis, D. N, and Dec, J. E., 2003, "Homogeneous Charge Compression Ignitions (HCCI) Engines: Key Research and Development Issues," SAE International, PT-94

[3] Epping, K., Aceves, S., Bechtold, R. and Dec, J., 2002, "The Potential of HCCI Combustion for High Efficiency and Low Emissions," SAE Technical Paper 2002-01-1923

[4] Zhao, H., Peng, Z., Williams, J., Ladommatos, N., 2001, "Understanding the Effects of Recycled Gases on the Controlled Autoignition (CAI) Combustion in Four-Stroke Gasoline Engines." SAE Paper No.2001- 01-3607

[5] Dec, J. E., 2002, "A Computational Study of the Effects of Low Fuel Loading and EGR on Heat Release Rates and Combustion Limits in HCCI Engines," SAE Paper NO. 2002-01-1309

[6] Caton, P. A., Song, H. H., Kaahaaina N. B. and Edwards, C. F., 2005, "Strategies for Achieving Residual-Affected Homogeneous Charge Compression Ignition using Variable Valve Actuation," SAE Paper NO. 2005-01-0165

[7] Law, D., Kemp, D., Allen, J., Kirkpatrick, G., and Copland, T., 2001, "Controlled Combustion in an IC-Engine with a Fully Variable Valve Train," SAE Paper No. 2001-01-0251

[8] Marriott, C. D, and Reitz, R. D., 2002, "Experimental Investigation of Direct Injection Gasoline for Premixed Compression Ignited Combustion Phasing Control," SAE Paper NO. 2002-01-0418

[9] Sjoberg, M., Edling, L. O., Eliassen, T., Magnusson, L. and Angstrom, H. E., 2002, "GDI HCCI: Effects of Injection Timing and Air-Swirl on Fuel Stratification Combustion and Emissions Formation." SAE Paper NO. 2002-01-0106

[10] Mikalsen, R. and Roskilly, A. P., 2007, "A Review of Free-piston Engine History and Applications," Applied Thermal Engineering, 27(14-15), pp.2339-2352

[11] Zhang, C., Li, K. and Sun, Z., 2015, "Modeling of Piston Trajectory-based HCCI Combustion Enabled by a Free Piston Engine," Applied Energy, 139(1), pp. 313-326

[12] Zhang, C. and Sun, Z., 2016, "Using Variable Piston Trajectory to Reduce Engine-out Emissions," Applied Energy, 170(1), pp. 403-313

[13] Zhang, C. and Sun, Z., 2017, "Trajectory-based Combustion Control for Renewable fuels in Free Piston Engines," Applied Energy, 187(1), pp. 72-83

[14] Li, K., Sadighi, A., and Sun, Z., 2014, "Active Motion Control of a Hydraulic Free Piston Engine," IEEE/ASME Transaction. Mechatronics, 19(4), pp. 1148-1159

[15] Li, K., Zhang, C. and Sun, Z., 2015, "Precise Piston Trajectory Control for a Free Piston Engine," Control Engineering Practice, 34, pp. 30-38

[16] Zhang, C. and Sun, Z., 2016, "Optimization of Trajectory-based HCCI Combustion," Proceedings of Dynamic Systems Control Conference, Minneapolis MN, 2016

[17] J. Heywood, 1988, Internal Combustion Engine Fundamentals, McGraw-Hill

[18] Goodwin, D., Malaya N., and Speth. R., "Cantera: An Object-oriented Software for Chemical Kinetics, Thermodynamics and Transport Processes", available at https://code.google.com/p/cantera/

[19] Zhang, C. and Sun, Z, 2018, "A Control-Oriented Model For Trajectory-Based HCCI Combustion Control," Journal of Dynamic Systems, Measurement, and Control, Volume 140, Page 091013-1-091013-10, Sep. 2018, doi: 10.1115/1.4039664.

[20] Zhang, C. and Sun, Z., 2017, "A Framework of Control-oriented Reaction-based Model for Trajectory-based HCCI Combustion with Variable Fuels," Proceedings of Dynamic Systems Control Conference, Tysons Corner, VA, 2017

[21] Jones, W. P., and Lindstedt, R. P., 1988, "Global Reaction Schemes for Hydrocarbon Combustion," Combustion and Flame, 73(3), pp. 233-249

[22] Bowman, C. T., 1975, "Kinetic of Pollutant Formation and Destruction in Combustion," Progress in Energy Combust. Sci., 1(1), pp. 33-45